

# BROKEN-RAY VIDEOMETRIC METHOD AND SYSTEM FOR MEASURING THE THREE-DIMENSIONAL POSITION AND POSE OF THE NON-INTERVISIBLE OBJECT

Qifeng YU <sup>a,b</sup>, Guangwen JIANG <sup>a</sup>, Sihua FU <sup>a</sup>, Yang SHANG <sup>b</sup>, Yonghui LIANG <sup>a</sup>, Lichun LI <sup>b</sup>

<sup>a</sup> College of Optoelectronic Science and Engineering, National University of Defense Technology, Changsha, Hunan, 410073, P. R. -China - yuqifeng@vip.sina.com,- jianggwen@hotmail.com,- fusihua2002cn@hotmail.com, - yonghuiliang@sina.com

<sup>b</sup> College of Aerospace and Material Engineering, National University of Defense Technology, Changsha, Hunan, 410073, P. R.- China - shangyang1977163@163.com, -Lichunmail@163.com

Commission V, WG V/1

**KEY WORDS:** Close Range Photogrammetry, Deformation, Digital photogrammetry, Simulation, Industrial measurement, Three-dimensional

## ABSTRACT:

The traditional videometrics technique is usually adopted to measure the relative position and pose between the intervisible objects, and is invalid for measuring the three-dimensional position, pose and deformation of the non-intervisible target. An innovative broken-ray videometrics method is proposed to resolve the non-intervisible measurement problem. Broken-ray path is constructed by relay-stations, each of which consists of camera(s) and/or marker(s). By processing the images sequence, the position, pose and real-time dynamic deformation can be measured, and then the errors subjected to the deformation can be compensated if needed. Finally, laboratory experiments are designed and implemented which show satisfactory accuracy. The broken-ray videometric system will play an important role in the crucial science and technology fields such as deformation measurement and dynamic analysis of large vessels, and deformation monitoring of tunnel country rock.

## 1. INTRODUCTION

The photogrammetry or videometrics has broad application fields for its advantages as high-precision, non-contact and low-cost. However, the traditional videometrics technique is usually adopted to measure the relative position and pose between the intervisible objects, and is invalid for measuring the three-dimensional position, pose and deformation between the non-intervisible targets.

In the civil field, the deformation of tunnel country rock needs to be measured and monitored during the construction of the tunnels, railways and wells. The non-intervisible points can be measured by GPS or auto-total station system by setting medium control points on the obstacles, or being transferred by several stations. However, these methods which can only provide the point position of the target to be measured are not able to provide the three-dimensional position and pose information.

In the military field, ship deformation in the large vessels or submarines caused by motion disturbances, sea waves, helm's operation, etc., would reduce the performance of observing and weapon systems. Since a large vessel is a huge structure and the distance between two positions on the vessel where the displacement and angular variation we are interested in is usually in a large scale, the traditional deformation measurement techniques normally are not suitable for the measurement of ship's deformation because they only measure local deformation, such as strain gauges, various interferometric techniques. Russian researchers (Mochalov, 2002) used two three-axis laser gyros unit and Kalman filter to measure the angular deformation. Many researchers used strain gauges,

Fiber Bragg Gratings (Baldwin, 2002; Kiddy, 2005; Pran, 2002) and accelerometers to measure the strain of key positions but the globe deformation needs an exact transform model that is difficult to derive.

In the application fields referred above, the target to be measured is often non-intervisible for the complex structure. For example, Inertial Navigation System (INS) is under the deck whereas the device to be measured is on the deck. The traditional photogrammetry, therefore, is invalid in this case. To solve this non-intervisible measurement problem, the concept of "broken-ray videometrics" is proposed in this paper. Broken-ray path is constructed by using relay-stations each of which is consisted of camera(s) and/or marker(s). This novel method has strong manoeuvrability and high accuracy.

The remainder of this article is organized as follows:

Section 2 proposes the principle of broken-ray videometrics used to measure the position and pose of the non-intervisible target.

Section 3 designs the laboratory experiment, and provides the experimental result. Finally, Section 4 puts forward some conclusions.

## 2. PRINCIPLE OF BROKEN-RAY VIDEOMETRICS

### 2.1 Reference Coordinate Systems and Notation

In this work, we propose to establish the measurement relay-stations to avoid the obstacles in the linear path and relay the position and pose of each station. As an example, only two relay-stations are concerned as shown in Figure1. The first relay-station is composed of two cameras, and the second is

composed of a camera and a marker which has cooperated symbols. It is assumed that the base reference  $B$  and the target  $G$  are non-intervisible, so the traditional videometrics is invalid.

The following reference coordinate systems are first defined: Base Reference System ( $B$ -RS) as the base reference; Cameral Reference System ( $C1$ -RS) and Camera2 Reference System ( $C2$ -RS) fixed together to compose the first relay-station; Marker Reference System ( $M$ -RS) and Camera3 Reference System ( $C3$ -RS) fixed together to compose the second relay-station; and last, tarGet Reference System ( $G$ -RS) to be measured.

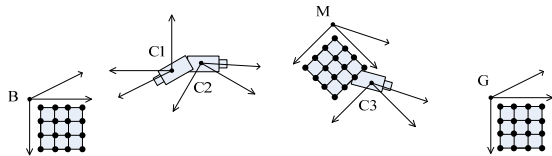


Figure 1 Reference Coordinate Systems

Within this study, points are expressed using 3D coordinates and are denoted with a capital letter and a left superscript indicating the reference system in which the point is expressed. For example, a point  $P$  expressed in the base reference system, has the coordinate  ${}^B P = [x, y, z]^T$ , where the right 'T' superscript indicates transposition. Given a point  ${}^I P$  expressed in an initial reference system, the corresponding coordinates expressed in the final reference system are related by a rigid transformation as:

$${}^F P = {}^F R_I {}^I P + {}^F T_I, \quad (1)$$

where  ${}^F R_I$  is the (3×3) rotation matrix denoted with a capital  $R$ ,  ${}^F T_I$  is the (3×1) translation vector denoted with a capital  $T$ , with a right subscript indicating the 'initial' reference system and a left superscript indicating the 'final' reference system.

## 2.2 Broken-ray Principle

The objective is to obtain the relative pose between the non-intervisible target and the base, i.e.  ${}^G R_B$  and  ${}^G T_B$ . From (1), we can conclude

$${}^{C1} P = {}^{C1} R_B {}^B P + {}^{C1} T_B \quad (2)$$

$${}^{C2} P = {}^{C2} R_{C1} {}^{C1} P + {}^{C2} T_{C1} \quad (3)$$

Then,  ${}^{C2} P$  can be expressed as, using (2) and (3),

$${}^{C2} P = {}^{C2} R_{C1} {}^{C1} R_B {}^B P + ({}^{C2} R_{C1} {}^{C1} T_B + {}^{C2} T_{C1}) \quad (4)$$

Analogously,  ${}^G P$  can be formulated as

$$\begin{aligned} {}^G P = & {}^G R_{C3} {}^{C3} R_M {}^M R_{C2} {}^{C2} R_{C1} {}^{C1} R_B {}^B P \\ & + {}^G R_{C3} {}^{C3} R_M {}^M R_{C2} {}^{C2} R_{C1} {}^{C1} T_B + {}^G R_{C3} {}^{C3} R_M {}^M R_{C2} {}^{C2} T_{C1} \quad (5) \\ & + {}^G R_{C3} {}^{C3} R_M {}^M T_{C2} + {}^G R_{C3} {}^{C3} T_M + {}^G T_{C3} \end{aligned}$$

In another way, the transformation of  $G$ -RS and  $B$ -RS can be expressed as

$${}^G P = {}^G R_B {}^B P + {}^G T_B \quad (6)$$

Compared with (5), the position and pose between the target and the base can be expressed as

$${}^G R_B = {}^G R_{C3} {}^{C3} R_M {}^M R_{C2} {}^{C2} R_{C1} {}^{C1} R_B \quad (7)$$

$$\begin{aligned} {}^G T_B = & {}^G R_{C3} {}^{C3} R_M {}^M R_{C2} {}^{C2} R_{C1} {}^{C1} T_B + {}^G R_{C3} {}^{C3} R_M {}^M R_{C2} {}^{C2} T_{C1} \quad (8) \\ & + {}^G R_{C3} {}^{C3} R_M {}^M T_{C2} + {}^G R_{C3} {}^{C3} T_M + {}^G T_{C3} \end{aligned}$$

where  ${}^{C2} R_{C1}$ ,  ${}^{C2} T_{C1}$  represent the transformation between the camera  $C1$  and  $C2$ , and  ${}^{C3} R_M$ ,  ${}^{C3} T_M$  represent the transformation between the Camera  $C3$  and the marker  $M$  which the camera is located,  ${}^{C1} R_B$ ,  ${}^{C1} T_B$ ,  ${}^M R_{C2}$ ,  ${}^M T_{C2}$ ,  ${}^G R_{C3}$  and  ${}^G T_{C3}$ , represent the transformation between the object  $B$ ,  $M$  or  $G$  and the camera  $C1$ ,  $C2$  or  $C3$  correspondingly.

In (7) and (8),  ${}^{C2} R_{C1}$ ,  ${}^{C2} T_{C1}$ ,  ${}^{C3} R_M$  and  ${}^{C3} T_M$  can be calibrated with other methods, such as the hand-eye calibration (Shiu, 1989; Park, 1994) in robotics to a certain extent;  ${}^{C1} R_B$ ,  ${}^{C1} T_B$ ,  ${}^M R_{C2}$ ,  ${}^M T_{C2}$ ,  ${}^G R_{C3}$  and  ${}^G T_{C3}$  can be calculated with the pose estimation algorithm (Lu, 2000; Ansar, 2003; Campa, 2006) from the information of 3D reference cooperative symbols expressed in object coordinates and their 2D projections expressed in the image coordinates. That is to say, all terms in (7) and (8) can be calibrated or calculated, hence the position and pose between the non-intervisible target and base is obtained.

From (7), we can also see that the rotation matrix is related to the mediate rotation matrices, being independent of the mediate translation vectors. In the case only the rotation angles are concerned, the computation work is reduced.

We have given the example with only two relay-stations, and the similar conclusions can be obtained with more relay-stations:

$${}^n R_0 = \prod_{i=0}^{n-1} {}^{n-i} R_{n-i-1} = {}^n R_{n-1} {}^{n-1} R_{n-2} \cdots {}^1 R_0 \quad (9)$$

$${}^nT_0 = {}^nT_{n-1} + \sum_{i=0}^{n-2} \left[ \left( \prod_{j=i+1}^{n-1} {}^{n-j}R_{n-j-1} \right) {}^{i+1}T_i \right] \quad (10)$$

where  ${}^{i+1}R_i$  and  ${}^{i+1}T_i$  represent the transformation of the  $i$ -th reference system and the  $(i+1)$ -th reference system. The multiplication sequence must be cared since the matrices multiplication is not exchangeable.

If the points are expressed using homogeneous (4D) coordinates such as  ${}^B P = [x, y, z, 1]^T$ , and the transformation matrices are (4×4) matrices such as  ${}^F M_I$ , then

$${}^F M_I = \begin{bmatrix} {}^F R_I & {}^F T_I \\ 0 & 1 \end{bmatrix} \quad (11)$$

Using (11), the equations (9), (10) can be reformulated as

$${}^n M_0 = \prod_{i=0}^{n-1} {}^{n-i} M_{n-i-1} = {}^n M_{n-1} {}^{n-1} M_{n-2} \cdots {}^1 M_0 \quad (12)$$

where  ${}^{i+1}M_i$  represent the (4×4) transformation matrix of the  $i$ -th reference system and the  $(i+1)$ -th reference system.

### 2.3 Broken-ray Relay Form

The broken-ray method is well-suited for many situations, for the relay form is various. The relay-station could be a camera and a marker fixed together as shown in Figure 1 (C3-M), or two cameras fixed together, as shown in Figure 1(C1-C2) and Figure 2(C1-C2, C3-C4). Furthermore, the relay-station could be one marker, as shown in Figure 2 (M). With these three types of relay-station, the relay form can be suited for any case.

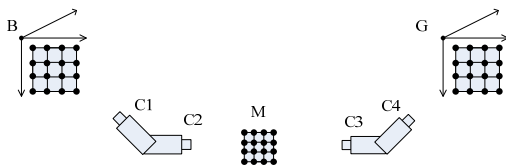


Figure 2 Broken-ray relay forms with three relay-stations

## 3. LABORATORY EXPERIMENTS

### 3.1 Experiments Setup

Laboratory experiments are designed and implemented. The real setup shown in Figure3 is a simple broken-ray relay form containing the base reference  $B$ , the target  $G$  and two relay-stations – one (C1-C2) consists of two cameras C1 and C2, the other (M-C3) consists of a marker  $M$  and a camera C3. The components in each relay-station, such as C1 and C2, are connected rigidly.

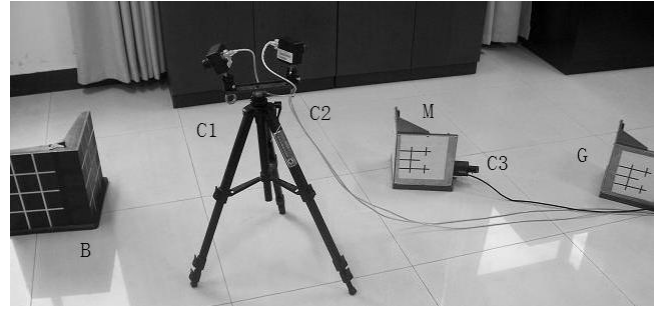


Figure 3 Real experiment setup

Camera C1 and C2 are two MVC1000Ms cameras with the resolution of 1280×1024 pixels, and C3 is one AVT camera with the resolution of 1392×1040. The base (B), marker (M) and target (G) are three objects with cooperative symbols. The geometry of the symbols is known as they were designed in the laboratory.

### 3.2 Experiments Steps

It is evident that the transformation of the  $B$ -RS and  $G$ -RS is invariable when the base and the target are fixed unmovable on the ground. Hence, the relay result of the transformation of  $B$ -RS and  $G$ -RS by the relay-stations must be a fixed value wherever the relay-stations stay.

The experiments are carried out with the following steps:

Step 1: Calibrate the internal parameters of the three cameras, including both lens distortion and the mapping from metric to pixel coordinates.

Step 2: Calibrate the relay-stations to get the information of the relative pose and position -  ${}^{C2}R_{C1}$ ,  ${}^{C2}T_{C1}$  between the two cameras in the first relay-station C1-C2, and  ${}^M R_{C3}$ ,  ${}^M T_{C3}$  between the marker and camera in the second relay-station M-C3.

Step 3: Acquire 3 images (or being called as one group of images) of 3 cameras and process them to get the position and pose information  ${}^{C1}R_B$ ,  ${}^{C1}T_B$ ,  ${}^M R_{C2}$ ,  ${}^M T_{C2}$ ,  ${}^G R_{C3}$  and  ${}^G T_{C3}$ .

Step 4: Rotate and/or move the relay-stations for several times, and acquire groups of images to get the positions and poses when the relay-stations stay at different conditions.

Step 5: Calculate  ${}^G R_B$  and  ${}^G T_B$  with the information of the calibrated data and processed data in the steps above.

Step 6: Compare and process the results.

### 3.3 Experimental Results

According to the steps mentioned in Section 3.2, we acquired more than 100 groups of images and got corresponding groups of  ${}^G R_B$ ,  ${}^G T_B$ . Only part of original data and the statistical result are shown in Table 4 and Table 5.

	A_x / deg	A_y / deg	A_z / deg
No.1	-4.1106	1.4515	164.4249
No.2	-4.1247	1.5001	164.4373
No.3	-4.1231	1.5011	164.4326
No.4	-4.1195	1.5339	164.4173
No.5	-4.1043	1.5008	164.413
No.6	-4.1294	1.5051	164.4842
No.7	-4.106	1.4553	164.4531
No.8	-4.1058	1.4557	164.4731
Min	-4.1294	1.4515	164.413
Max	-4.1043	1.5339	164.4842
Ave	-4.11543	1.4879	164.4419
Rms	0.009256	0.02812	0.02430

Table 4 Results of rotation angles

	T_x / mm	T_y / mm	T_z / mm
No.1	-1282.9398	-2952.0529	532.8236
No.2	-1283.5764	-2951.5021	531.9766
No.3	-1283.5592	-2951.4957	531.8821
No.4	-1283.6027	-2951.4567	531.3036
No.5	-1283.6827	-2951.3879	532.3849
No.6	-1283.7936	-2952.4626	531.8462
No.7	-1282.7306	-2951.9466	533.1364
No.8	-1281.5911	-2955.1939	534.1465
Min	-1283.7936	-2955.1939	531.3036
Max	-1281.5911	-2951.3879	534.1465
Ave	-1283.1845	-2952.1873	532.4374
Rms	0.6976	1.1891	0.8454

Table 5 Results of translations

In Table 4 and Table 5, A\_x, A\_y, A\_z represent the pose – three Euler angles in degree, T\_x, T\_y, T\_z represent the position – three components of the translation vector in millimeter. Min, Max, Ave, Rms mean the minimum value, the maximum value, the average value and the root of mean square of the data derivation.

The experimental results show that the proposed method has a high degree of accuracy. The rotation angle's error is about 70 angular seconds in average, when the translation vector's error depending on the rotation matrix and the imaging distance is less than 1.5 mm in the laboratory experiment. With higher resolution cameras and advanced calibration and pose estimation methods, the accuracy can be improved.

#### 4. CONCLUSIONS

Measurement of the three-dimensional position and pose of the non-intervisible object is very difficult task in large scale structures. Since conventional deformation measurement techniques are not suitable for the case, we present an innovative broken-ray videometrics method to resolve this problem.

The broken-ray method can measure three-dimensional position and pose of non-intervisible target, and is also valid for the intervivable target. The broken-ray system has the capability to work continuously, giving the dynamic and real-time three-dimensional position and pose. Laboratory experiments show the satisfactory accuracy.

The research on broken-ray videometrics can not only solve the problem of measuring three-dimensional position, pose and deformation between non-intervivable objects, but also promote the progress of the videometric technique and expand its application fields. The broken-ray videometrics method proposed are very promising and will play an important role in the crucial science and technology fields such as deformation measurement, stress analysis, and structural monitoring.

#### ACKNOWLEDGEMENT

Partial support for the authors has been provided by the National Natural Science Foundation of China (Project 10727202).

#### REFERENCE

- Mochalov, A., 2002. Use of the ring laser units for measurement of the moving object deformation. In: *Proceedings of SPIE*, Vol. 4680, pp. 85-92.
- Baldwin, C., 2002. Fiber optic structural health monitoring system: rough sea trials testing of the RV Triton. In: *Oceans 2002, Proceedings of MTS/IEEE*, Vol.3, pp. 1806-1813.
- Kiddy, J., 2005. Hydrostatic Testing of a Manned Underwater Vehicle using Fiber Optic Sensors. In: *Oceans 2005, Proceedings of MTS/IEEE*, pp. 1-6.
- Pran, K., 2002. Instrumentation of a high-speed surface effect ship for structural response characterisation during seatrials. In: *Proceedings of SPIE*, Vol. 3986, pp. 372-379.
- Shiu, Y., 1989. Calibration of Wrist-Mounted Robotic Sensors by Solving Homogeneous Transform Equations of the Form AX=XB. *IEEE Transactions on Robotics and Automation*, Vol. 5, No. 1, pp. 16-29.
- Park, F., 1994. Robot Sensor Calibration: Solving AX=XB on the Euclidean Group. *IEEE Transaction on Robotics and Automation*, Vol. 10, No. 5, pp. 717-721.
- Lu, C., 2000. Fast and globally convergent pose estimation from video images. *IEEE Transactions on Pattern Analysis and Machine Intelligence*, Vol. 22, No. 6, pp. 610-622.
- Ansar, A., 2003. Linear pose estimation from points or lines. *IEEE Transactions on Pattern Analysis and Machine Intelligence*, Vol. 25, No. 5, pp. 578-589.
- Campa, G., 2006. A comparison of Pose Estimation algorithms for Machine Vision based Aerial Refueling for UAVs. In: *MED'06, 14th Mediterranean Conference on Control and Automation*, pp. 1-6.